Eur. Phys. J. A **26**, 241–251 (2005)
DOI 10.1140/epja/i2004-10308-1

THE EUROPEAN PHYSICAL JOURNAL A

Fusion near the Coulomb barrier for the synthesis of heavy and superheavy elements: A theoretical approach

N. Bhatia[1], S.S. Malik[1,a], and A.K. Jain[2]

[1] Department of Physics, G.N.D. University, Amritsar-143005, India
[2] Department of Physics, Indian Institute of Technology Roorkee, Roorkee-247667, India

Received: 4 October 2004 / Revised version: 21 October 2005 /
Published online: 5 December 2005 –
Communicated by A. Molinari

Abstract. The compound nucleus formation is considered as a two-step process of touching and subsequent tunneling of the projectile into the target. The deep minima in the potential energy curve are due to shell effects in the experimental binding energies and give possible target-projectile combinations for the synthesis of heavy and superheavy elements. The asymmetric channels thus obtained are in remarkable agreement with the known experimental channels. In our model, the colliding partners are first shown to be captured in the pocket behind the outer (touching) barrier and the composite system so formed finally tunnels through the inner (fusion) barrier to form the resulting compound nucleus. These calculations reveal the importance of the fusion barrier, which occur only for the asymmetric target-projectile combinations. The calculated fusion cross-sections show a reasonable comparison with the observed one-neutron evaporation residue cross-sections. An estimate of the excitation energy carried by the compound nucleus is also obtained from our model calculations.

PACS. 24.10.-i Nuclear-reaction models and methods – 25.70.Gh Compound nucleus – 25.70.Jj Fusion and fusion-fission reactions – 25.60.Pj Fusion reactions

1 Introduction

Formation of new elements became a reality in the middle of the last century, when Fermi and coworkers bombarded an uranium target with neutrons. This led to the formation of new elements beyond $Z = 92$ through neutron capture with subsequent β-decay. This method achieved a remarkable success in the production of heavy elements till $Z = 100$ was reached, where spontaneous fission terminated the periodic table. This termination limit gave birth to a new era of the formation of heavy and superheavy elements (SHE) with heavy-ion beams. Beams ranging from α-particle upto ^{86}Kr and targets as heavy as ^{208}Pb and heavier radioactive nuclei have now been used to form elements with a maximum nuclear charge $Z = 116$ [1–6].

Mainly, two types of fusion processes are known for the synthesis of SHE, namely, above and below the Coulomb barrier. The former approach uses transuranium targets and involves the formation of compound nuclei with excitation energy large enough to evaporate ~ 3 nucleons before reaching the ground state. The latter approach (hereafter referred to as fusion process II) aims to use closed-shell target-projectile combinations to form the compound nuclei with low excitation energy, such that only ~ 1 neutron may be evaporated. In this fusion process, the enhanced cross-section is observed at an incident energy below the interaction barrier.

In this paper, the fusion process II is considered as a two-step quantum-mechanical process of touching and subsequent tunneling of the projectile into the target. Here, the most appropriate channels (*i.e.* target-projectile combinations) are located from the deep minima in the potential energy curve. We use the asymmetric two-center shell model (ATCSM) [7–12] for calculating the adiabatic interaction potential for the symmetric as well as the asymmetric channels. In case of asymmetric channels the fusion barriers are seen, which are penetrated to form the compound nuclei. Within our model calculations, we are able to get an estimate of the excitation energy carried by the compound nucleus.

We would like to point out that the two-step model proposed by Shen *et al.* [13] is based on statistical theory and is applicable to the hot-fusion process.

A complete model is presented in sect. 2. Section 3 highlights the results and discussion. Finally, conclusions are presented in sect. 4.

[a] e-mail: shammalik@yahoo.com

2 The model

Since the compound-nucleus formation is a two-step process, it involves a knowledge of i) the preformation (touching) probability, P_{CN} and ii) the tunneling probability, P_R, of the confining nuclear interaction barrier. Both these quantities are obtained by using a dynamical theory, based on the ATCSM. We introduce the relevant degrees of freedom of mass and charge asymmetries of two fragments,

$$\eta_A = \frac{(A_1 - A_2)}{A}, \quad \text{and} \quad \eta_Z = \frac{(Z_1 - Z_2)}{Z}, \qquad (1)$$

in addition to the usual coordinates of relative separation, $\vec{R}$, deformations of the colliding nuclei, β_i $(i = 1, 2)$, and the neck parameter, ϵ.

In principle, these two steps, involving η_A (or η_Z) and R are coupled. The stationary Schrödinger equation in the coupled η $(= \eta_A$ or $\eta_Z)$ and R can be written as

$$H(\eta, R)\Psi^\nu(\eta, R) = E^\nu \Psi^\nu(\eta, R). \qquad (2)$$

Here, the quantum number $\nu = 0, 1, 2, \ldots$ counts the vibrational states Ψ^ν in the potential. However, it has already been shown that the coupling effects of R to η in the potential are very small, at least for the fission charge distribution [14] and α-particle transfer resonances [15]. Also, it is known that the cranking coupling masses $B_{R\eta_A}$ and $B_{R\eta_Z}$ are very small such that $B_{R\eta_A} \ll \sqrt{B_{RR}B_{\eta_A\eta_A}}$ and $B_{R\eta_Z} \ll \sqrt{B_{RR}B_{\eta_Z\eta_Z}}$ hold good [11,16]. Furthermore, an experimental support for this assumption is also given in ref. [17], at least for the nuclear charge, indicating that the division of the nuclear charge is decided much earlier than for neutrons, so that on the way to scission the two nascent fragments are polarized by the Coulomb repulsion and they are linked by a neutron-rich neck. In view of these results, the Schrödinger equation (2), within decoupled approximation

$$\Psi^\nu(\eta, R) = \psi^\nu(\eta)\phi^\nu(R) \qquad (3)$$

separates into the following two equations:

$$\left[-\frac{\hbar^2}{2\sqrt{B_{\eta\eta}}}\frac{\partial}{\partial\eta}\left(\frac{1}{\sqrt{B_{\eta\eta}}}\frac{\partial}{\partial\eta}\right) + V(\eta)\right]\psi^\nu(\eta) = {E_1}^\nu \psi^\nu(\eta), \qquad (4)$$

$$\left[-\frac{\hbar^2}{2\sqrt{B_{RR}}}\frac{\partial}{\partial R}\left(\frac{1}{\sqrt{B_{RR}}}\frac{\partial}{\partial R}\right) + V(R)\right]\phi^\nu(R) = {E_2}^\nu \phi^\nu(R), \qquad (5)$$

with

$$E^\nu = {E_1}^\nu + {E_2}^\nu. \qquad (6)$$

2.1 The preformation probability, P_{CN}

Consider the first step of the fusion process II, wherein we calculate the compound-nucleus preformation probability, P_{CN}. This quantum-mechanical probability of selecting the fragments A_1 and A_2 (with fixed charge asymmetry, η_Z) at a fixed point R of the relative motion is obtained by solving eq. (4). It is solved numerically at the touching configuration R_t $(= R_1 + R_2$, R_i being radii of two colliding partners). At this configuration, the collective potential can be expressed simply as

$$V(\eta)\mid_{R_t} = -B_1(A_1, Z_1) - B_2(A_2, Z_2) + E_C + V_P\,. \qquad (7)$$

Here, A_i, Z_i $(i = 1, 2)$ are fixed by minimizing in the charge asymmetry, the sum of the two binding energies, $B_i(A_i, Z_i)$ (taken from ref. [18] in terms of their mass excess), the Coulomb interaction E_C $(= \frac{Z_1 Z_2 e^2}{R_t})$ and the proximity potential, V_P (which is calculated by using the formalism of Blocki *et al.* [19]). In these calculations, we have varied the mass asymmetry, η_A, in step of two-nucleon transfer.

The mass parameters, $B_{\eta\eta}$, for the kinetic energy term in eq. (4) are calculated by using the model of Kroger and Scheid [20]. This classical model gives a simple analytical expression for the mass parameters, whose predictions are known to compare nicely with the microscopic calculations of Yamaji *et al.* [21].

Knowing the potential and mass parameters, eq. (4) is solved numerically. Then, $\mid \psi(\eta) \mid^2$ is the probability of finding the target-projectile combination at the position R_t, which when normalized gives the preformation probability

$$P_{CN} = \mid \psi(\eta) \mid^2 \sqrt{B_{\eta\eta}}\frac{4}{A}. \qquad (8)$$

Here, the normalization is numerically checked. If only the ground state contributes and there is a complete adiabaticity, then $\nu = 0$. However, if the system were excited or we allowed the effects of the interaction with other degrees of freedom, then higher values of ν would contribute. The possible consequences of such excitations are included here through the simple Boltzmann-like occupation of excited states

$$\mid \psi(\eta) \mid^2 = \frac{\sum_\nu \mid \psi^\nu \mid^2 \exp\left(-\frac{{E_1}^\nu}{\Theta}\right)}{\sum_\nu \exp(-\frac{{E_1}^\nu}{\Theta})}\,. \qquad (9)$$

Here, Θ is the nuclear temperature (in MeV) and is related to the excitation energy E^* by the following statistical expression [22]:

$$\Theta = \sqrt{\frac{10E^*}{A}} \qquad (10)$$

with $E^* = E_{cm} - Q$. Since the excitation energy in the fusion process II is small, we have considered only the ground-state preformation probability in our present calculations.

2.2 The tunneling probability, P_R

In the second step of our model, we have considered the fusion of two touching partners to form the resulting compound nucleus. The interaction potential, $V(R)$ in eq. (5), is calculated by using the ATCSM [16]. The ATCSM gives the total potential as a sum of the fluctuating part of the level density (the shell correction term) arising from the

Table 1. An adiabatic interaction potential, $V(R)$, and ATCSM parameters for $^{256}_{102}$No using the symmetric channel ^{124}Sn + ^{132}Te. Here, the units of lengths and energies are in Fermi and MeV, respectively.

λ	η	ϵ	β_1	β_2	z_1	z_2	a_1	a_2	b_1	b_2	Neck	R_{cm}	V_{LDM}	δu	δp
1.21	.0246	0.	1.34	1.26	−0.30	0.28	9.40	8.84	7.02	7.02	7.02	5.49	1804.1081	4.6249	−0.3709
1.225	.0257	0.	1.36	1.28	−0.34	0.32	9.48	8.92	6.97	6.97	6.97	6.78	1804.1483	2.9987	−1.7259
1.25	.0331	0.	1.38	1.30	−0.54	0.51	9.48	8.92	6.87	6.86	6.87	7.04	1804.2047	−0.7216	1.0432
1.30	.0265	0.	1.39	1.32	−1.14	1.08	9.25	8.75	6.65	6.63	6.64	8.00	1804.2499	−10.5972	1.8820
1.35	.0320	0.	1.31	1.24	−2.49	2.34	8.31	7.85	6.35	6.33	6.34	8.05	1804.0976	1.3102	0.0470
1.40	.0282	0.	1.21	1.17	−3.73	3.57	7.40	7.08	6.11	6.05	6.08	8.56	1803.5928	−2.3205	1.1396
1.425	.0305	0.	1.12	1.07	−4.70	4.47	6.66	6.33	5.95	5.92	5.92	8.87	1803.1860	−1.7979	0.8838
1.45	.0349	0.04	1.10	1.02	−5.25	4.89	6.43	5.99	5.84	5.87	5.78	9.13	1802.7374	−0.5617	0.2935
1.50	.0310	0.08	1.04	1.01	−5.90	5.66	6.01	5.77	5.77	5.71	5.51	9.67	1801.5241	1.1920	0.4242
1.55	.0304	0.10	0.95	0.92	−6.91	6.62	5.40	5.18	5.68	5.63	5.17	10.60	1799.9150	1.6422	1.1325
1.629	.0237	1.00	1.00	1.00	−6.40	6.27	6.40	6.27	6.40	6.27	0.0729	13.31	1824.1297	−10.5216	0.5379
2.20	.0274	1.00	1.00	1.00	−10.85	10.63	6.44	6.31	6.44	6.31	0.00	22.3	1681.3493	−10.5294	0.7573

Table 2. An adiabatic interaction potential, $V(R)$, and ATCSM parameters for $^{256}_{102}$No using the asymmetric channel ^{48}Ca + ^{208}Pb. Here, the units of lengths and energies are in Fermi and MeV, respectively.

λ	η	ϵ	β_1	β_2	z_1	z_2	a_1	a_2	b_1	b_2	Neck	R_{cm}	V_{LDM}	δu	δp
1.20	.626	0.	1.59	0.57	−3.10	0.96	11.15	3.45	7.02	6.06	6.25	7.10	1807.5246	−4.1931	1.6059
1.25	.626	0.	1.68	0.61	−3.26	1.02	11.56	3.61	6.88	5.91	6.11	7.39	1807.3628	2.1074	0.0686
1.30	.624	0.	1.78	0.64	−3.45	1.07	11.99	3.72	6.73	5.81	5.99	7.74	1807.1693	6.1389	−1.5779
1.35	.621	0.	1.83	0.67	−3.92	1.23	12.07	3.79	6.59	5.65	5.84	8.13	1806.9355	3.2905	0.0944
1.40	.623	0.	1.91	0.70	−4.23	1.33	12.34	3.88	6.46	5.54	5.72	8.43	1806.6478	0.8867	0.6234
1.45	.617	0.	1.60	0.64	−6.94	2.31	9.98	3.32	6.24	5.19	5.40	9.18	1806.0897	0.4128	0.9860
1.50	.619	0.	1.54	0.65	−7.92	2.73	9.43	3.25	6.12	5.01	5.23	9.65	1805.4018	0.8818	0.1403
1.55	.621	0.	1.38	0.57	−9.82	3.34	8.17	2.78	5.92	4.88	5.09	10.30	1804.3646	1.8154	0.1726
1.567	.619	1.00	1.00	1.00	−7.55	4.63	7.55	4.63	7.55	4.63	0.001	12.94	1841.0534	−12.3206	2.2663
2.40	.625	1.00	1.00	1.00	−15.47	9.49	7.67	4.70	7.67	4.70	0.00	25.70	1793.0726	−15.4701	2.3177

Table 3. An adiabatic interaction potential, $V(R)$, and ATCSM parameters for $^{258}_{104}$Rf using the symmetric channel ^{122}Sn + ^{136}Xe. Here, the units of lengths and energies are in Fermi and MeV, respectively.

λ	η	ϵ	β_1	β_2	z_1	z_2	a_1	a_2	b_1	b_2	Neck	R_{cm}	V_{LDM}	δu	δp
1.19	.0458	0.	1.33	1.20	−0.33	0.30	9.44	8.50	7.10	7.09	7.09	6.43	1856.7516	10.1293	−3.5735
1.25	.0741	0.	1.41	1.27	−0.55	0.50	9.71	8.74	6.89	6.88	6.88	7.82	1856.8080	−7.7307	1.2598
1.30	.0450	0.	1.38	1.26	−1.48	1.34	9.15	8.31	6.63	6.59	6.61	8.05	1856.7252	−11.6879	2.0181
1.35	.0540	0.	1.24	1.14	−3.21	2.92	7.81	7.12	6.30	6.24	6.27	8.19	1856.3624	−0.1965	0.8364
1.40	.0514	0.	1.17	1.09	−4.25	3.91	7.12	6.55	6.09	6.01	6.05	8.66	1855.5935	−2.1500	0.9294
1.45	.0507	0.04	1.07	1.02	−5.36	5.01	6.33	5.92	5.92	5.80	5.77	9.19	1854.4726	−1.0877	0.7100
1.475	.0563	0.07	1.07	0.98	−5.81	5.29	6.24	5.67	5.83	5.79	5.63	9.47	1853.7664	−0.2489	0.7454
1.50	.0542	0.08	0.94	0.89	−6.68	6.22	5.44	5.06	5.79	5.68	5.37	10.00	1852.9258	1.3320	1.0969
1.55	.0504	0.11	0.93	0.89	−7.14	6.69	5.34	5.01	5.75	5.63	5.10	10.80	1851.0141	1.2861	1.0189
1.631	.0415	1.00	1.00	1.00	−6.47	6.24	6.47	6.24	6.47	6.24	0.0001	13.36	1875.0289	−8.0520	0.7497
2.40	.0464	1.00	1.00	1.00	−12.57	12.13	6.48	6.25	6.48	6.25	0.00	25.5	1737.8455	−8.7065	1.1191

Table 4. An adiabatic interaction potential, $V(R)$, and ATCSM parameters for $^{258}_{104}$Rf using the asymmetric channel ^{50}Ti + ^{208}Pb. Here, the units of lengths and energies are in Fermi and MeV, respectively.

λ	η	ϵ	β_1	β_2	z_1	z_2	a_1	a_2	b_1	b_2	Neck	R_{cm}	V_{LDM}	δu	δp
1.20	.614	0.	1.59	0.57	−3.10	0.97	11.15	3.50	7.01	6.14	6.32	7.11	1860.0925	−3.7997	−1.5626
1.25	.615	0.	1.69	0.61	−3.20	1.01	11.62	3.66	6.88	6.01	6.18	7.39	1859.8247	2.7123	−0.3059
1.30	.613	0.	1.79	0.64	−3.39	1.06	12.05	3.78	6.73	5.90	6.07	7.74	1859.5126	5.9744	−1.4986
1.32	.610	0.	1.78	0.65	−3.76	1.19	11.87	3.77	6.67	5.80	5.98	7.94	1859.3759	5.4398	−0.8169
1.35	.610	0.	1.83	0.67	−3.92	1.25	12.06	3.84	6.59	5.73	5.91	8.14	1859.1420	3.3890	0.1025
1.40	.610	0.	1.86	0.70	−4.48	1.45	12.01	3.89	6.45	5.56	5.75	8.49	1858.7098	−0.0323	1.1189
1.41	.610	0.	1.86	0.70	−4.66	1.51	11.94	3.87	6.42	5.53	5.72	8.56	1858.6117	−0.0892	1.0322
1.42	.604	0.	1.51	0.63	−6.90	2.40	9.53	3.31	6.31	5.26	5.48	9.04	1858.3756	0.6233	0.9024
1.425	.604	0.	1.51	0.63	−6.98	2.43	9.51	3.30	6.30	5.24	5.46	9.08	1858.2946	0.5892	0.9549
1.45	.605	0.	1.48	0.64	−7.43	2.65	9.25	3.29	6.25	5.14	5.37	9.32	1857.8730	0.2112	0.5970
1.50	.606	0.	1.42	0.63	−8.50	3.08	8.68	3.14	6.11	4.99	5.22	9.78	1856.9410	−0.8575	0.4433
1.55	.593	0.	1.34	0.57	−8.90	3.59	8.32	3.36	6.12	4.73	5.03	10.19	1855.6258	−0.2823	0.4124
1.575	.615	1.0	1.00	1.00	−7.57	4.71	7.57	4.71	7.57	4.71	0.0001	13.03	1893.3430	−8.6498	2.1935
2.40	.628	1.0	1.00	1.00	−15.59	9.70	7.48	4.66	7.48	4.66	0.0	26.10	1797.7827	−12.7734	2.2668

Table 5. An adiabatic interaction potential, $V(R)$, and ATCSM parameters for $^{260}_{106}$Sg using the symmetric channel ^{122}Sn + ^{138}Ba. Here, the units of lengths and energies are in Fermi and MeV, respectively.

λ	η	ϵ	β_1	β_2	z_1	z_2	a_1	a_2	b_1	b_2	Neck	R_{cm}	V_{LDM}	δu	δp
1.20	.0824	0.	1.34	1.19	−0.49	0.44	9.46	8.38	7.06	7.04	7.05	6.41	1909.7666	11.2108	−7.9620
1.25	.0656	0.	1.38	1.23	−0.89	0.79	9.46	8.41	6.86	6.84	6.85	7.13	1909.6930	1.2530	−0.0129
1.30	.0638	0.	1.30	1.17	−2.22	1.98	8.51	7.61	6.55	6.51	6.53	7.73	1909.4878	4.6597	−0.5785
1.35	.0606	0.	1.23	1.13	−3.30	2.99	7.77	7.05	6.32	6.23	6.27	8.22	1908.8763	−1.0623	1.1815
1.40	.0594	0.	1.16	1.07	−4.40	4.00	7.07	6.43	6.10	6.01	6.05	8.68	1907.8740	−2.3262	1.2448
1.425	.0593	0.04	1.07	1.00	−5.21	4.78	6.41	5.88	5.99	5.88	5.85	9.03	1907.1744	−0.8166	0.6986
1.45	.0624	0.06	1.02	0.94	−5.86	5.33	6.02	5.47	5.90	5.82	5.69	9.37	1906.4087	0.4124	0.3804
1.475	.0601	0.08	0.96	0.92	−6.29	5.86	5.65	5.27	5.88	5.73	5.51	9.73	1905.5491	0.2953	0.8585
1.50	.0612	0.09	0.93	0.88	−6.77	6.26	5.42	5.01	5.83	5.70	5.34	10.1	1904.5078	1.3631	0.9671
1.55	.0522	0.10	0.82	0.78	−7.82	7.25	4.75	4.41	5.80	5.66	4.89	11.80	1902.1796	−2.2055	1.4350
1.631	.0502	1.00	1.00	1.00	−6.51	6.24	6.51	6.24	6.51	6.24	0.0001	13.39	1925.2219	−5.6790	0.2514
2.40	.0552	1.00	1.00	1.00	−12.64	12.13	6.51	6.25	6.51	6.25	0.00	25.5	1783.2808	−6.4197	0.9692

quantal shell correction and the liquid-drop energy, V_{LDM} (sum of the Coulomb and the surface energies) with the parameters of Myers and Swiatecki [23]. We define

$$V(R) = V_{LDM} + \delta u + \delta p, \tag{11}$$

where δu and δp are the shell and the pairing contributions, respectively.

Here, the adiabatic interaction potentials are calculated by carrying out a self-consistent minimization of the total energy (eq. (11)) in the shape parameters β_i $(i = 1, 2)$, ϵ and the dynamical mass asymmetry parameter, η_A. These potentials along with their shape parameters are given in tables 1-10 for both symmetric and asymmetric channels of five systems with Z = 102, 104, 106, 108 and 110. Also, we have plotted the interaction potential, $V(R)$, *vs.* the R_{cm} both for the asymmetric and the symmetric channels, respectively, in figs. 3 and 4 further on. In fig. 3, a double-humped barrier arises in each system, namely, the outer (touching) barrier and the inner (fusion) barrier. Whereas in fig. 4, no such double-humped barrier is seen. In the fusion process II, the incoming system gets captured in the pocket behind the touching barrier and subsequently tunnels through the fusion barrier to form a compound nucleus. For the penetration probability, P_R, we solve eq. (5) by using the WKB approximation with constant mass, *i.e.* $B_{RR} = \mu$ (μ being the reduced mass of the combination) and is given by

$$P_R = \exp\left[-\frac{2}{\hbar}\int_{R_i}^{R_f}\sqrt{2\mu(V(R) - V(R_i))}\mathrm{d}R\right]. \tag{12}$$

The first (inner) turning point in the WKB penetrability integral is chosen at $R_i = R_C$, the compound-nucleus

Table 6. An adiabatic interaction potential, $V(R)$, and ATCSM parameters for $^{260}_{106}$Sg using the asymmetric channel ^{54}Cr + ^{206}Pb. Here, the units of lengths and energies are in Fermi and MeV, respectively.

λ	η	ϵ	β_1	β_2	z_1	z_2	a_1	a_2	b_1	b_2	Neck	R_{cm}	V_{LDM}	δu	δp
1.20	.588	0.	1.55	0.58	−3.25	1.08	10.84	3.60	6.99	6.21	6.38	7.14	1912.9874	−2.3741	1.2030
1.25	.587	0.	1.62	0.62	−3.52	1.19	11.10	3.74	6.85	6.04	6.22	7.47	1912.5866	3.7763	−0.6147
1.275	.587	0.	1.67	0.63	−3.64	1.21	11.31	3.78	6.77	6.00	6.16	7.64	1912.3548	5.6472	−0.7972
1.30	.585	0.	1.71	0.65	−3.75	1.26	11.47	3.85	6.71	5.92	6.09	7.83	1912.1090	5.8632	−1.3366
1.35	.581	0.	1.73	0.68	−4.36	1.50	11.36	3.90	6.57	5.73	5.92	8.25	1911.5537	1.5764	0.7561
1.375	.577	0.	1.60	0.70	−5.29	1.95	10.42	3.84	6.51	5.49	5.71	8.56	1911.2262	0.4633	1.2642
1.40	.578	0.	1.60	0.71	−5.64	2.10	10.31	3.84	6.44	5.40	5.64	8.75	1910.8546	0.4146	1.1285
1.45	.580	0.	1.41	0.64	−7.68	2.90	8.78	3.32	6.23	5.18	5.42	9.37	1909.6871	−0.0962	0.3944
1.505	.581	0.00	1.24	0.55	−9.72	3.62	7.43	2.77	5.99	5.03	5.24	10.10	1908.2608	−1.7252	0.7845
1.55	.585	0.00	1.25	0.56	−10.26	3.84	7.37	2.76	5.90	4.93	5.15	10.6	1906.8925	−1.4690	1.3258
1.606	.574	1.00	1.00	1.07	−7.52	5.03	7.52	5.03	7.52	4.71	0.0001	13.29	1938.8603	−2.8143	−0.0523
2.40	.609	1.00	1.00	1.074	−15.00	10.06	7.46	5.01	7.46	5.01	0.00	25.80	1841.2310	−5.0103	1.2224

Table 7. An adiabatic interaction potential, $V(R)$, and ATCSM parameters for $^{266}_{108}$Hs using the symmetric channel ^{132}Xe + ^{134}Xe. Here, the units of lengths and energies are in Fermi and MeV, respectively.

λ	η	ϵ	β_1	β_2	z_1	z_2	a_1	a_2	b_1	b_2	Neck	R_{cm}	V_{LDM}	δu	δp
1.25	.0085	0.	1.32	1.30	−0.81	0.79	9.12	8.98	6.91	6.91	6.91	7.19	1954.8276	1.9874	−0.5051
1.30	.0077	0.	1.18	1.17	−2.61	2.58	7.69	7.61	6.52	6.50	6.51	7.88	1954.4878	4.2412	−0.6108
1.35	.0064	0.	1.13	1.13	−3.55	3.53	7.11	7.08	6.29	6.26	6.28	8.35	1953.6435	−1.0045	1.1632
1.40	.0061	0.	1.07	1.07	−4.55	4.53	6.51	6.47	6.08	6.05	6.06	8.81	1952.3939	−1.6676	1.0577
1.45	.0063	0.07	0.98	0.98	−5.65	5.62	5.81	5.78	5.93	5.89	5.71	9.47	1950.6561	−0.2726	0.8017
1.50	.0073	0.10	0.89	0.89	−6.65	6.62	5.20	5.17	5.84	5.81	5.32	10.34	1948.3953	−0.8074	1.2489
1.55	.0088	0.10	0.78	0.78	−7.72	7.68	4.53	4.50	5.80	5.77	4.87	12.09	1945.6107	−4.7025	0.5840
1.629	.0067	1.00	1.00	1.00	−6.43	6.40	6.43	6.40	6.43	6.40	0.1269	13.48	1966.8100	−6.2971	−0.3755
2.40	.0082	1.00	1.00	1.00	−12.51	12.44	6.45	6.41	6.45	6.41	0.00	25.7	1821.2930	−6.7573	0.0731

Table 8. An adiabatic interaction potential, $V(R)$, and ATCSM parameters for $^{266}_{108}$Hs using the asymmetric channel ^{58}Fe + ^{208}Pb. Here, the units of lengths and energies are in Fermi and MeV, respectively.

λ	η	ϵ	β_1	β_2	z_1	z_2	a_1	a_2	b_1	b_2	Neck	R_{cm}	V_{LDM}	δu	δp
1.20	.564	0.	1.58	0.63	−2.75	0.97	11.22	3.97	7.10	6.30	6.49	7.13	1958.0822	−3.1195	1.0510
1.25	.562	0.	1.60	0.68	−3.24	1.20	11.14	4.12	6.96	6.05	6.26	7.50	1957.6259	2.3965	−0.0057
1.275	.560	0.	1.52	0.65	−4.30	1.60	10.35	3.84	6.81	5.91	6.11	7.86	1957.3229	5.4984	−1.1989
1.30	.559	0.	1.54	0.66	−4.57	1.70	10.37	3.85	6.73	5.83	6.04	8.07	1956.9837	5.0045	−0.6797
1.35	.556	0.	1.58	0.69	−5.04	1.89	10.42	3.92	6.59	5.68	5.89	8.43	1956.2195	1.4697	1.3752
1.40	.559	0.	1.55	0.70	−5.94	2.29	9.99	3.84	6.45	5.49	5.71	8.83	1955.3259	−0.3106	1.5800
1.45	.559	0.	1.35	0.63	−7.99	3.14	8.41	3.31	6.23	5.25	5.48	9.48	1953.9038	−0.6669	0.9622
1.50	.561	0.00	1.19	0.55	−9.82	3.84	7.17	2.80	6.03	5.09	5.31	10.30	1952.3635	−2.7272	1.6181
1.55	.566	0.00	1.23	0.56	−10.35	4.00	7.27	2.81	5.91	5.02	5.22	10.7	1950.6157	−2.4305	1.6720
1.581	.536	1.00	1.00	1.00	−7.59	4.92	7.54	4.92	7.54	4.92	0.0001	13.19	1984.8329	−4.6162	0.7099
2.40	.563	1.00	1.00	1.00	−15.39	10.05	7.48	4.89	7.48	4.89	0.00	26.20	1877.1677	−4.5272	0.7430

Table 9. An adiabatic interaction potential, $V(R)$, and ATCSM parameters for $^{272}_{110}$X using the symmetric channel ^{132}Te + ^{140}Ce. Here, the units of lengths and energies are in Fermi and MeV, respectively.

λ	η	ϵ	β_1	β_2	z_1	z_2	a_1	a_2	b_1	b_2	Neck	R_{cm}	V_{LDM}	δu	δp
1.20	.0149	0.	1.30	1.24	−0.43	0.41	9.32	8.88	7.17	7.16	7.17	6.33	2000.6109	7.2117	0.7031
1.25	.0214	0.	1.31	1.25	−1.10	1.04	9.06	8.64	6.92	6.91	6.91	7.86	2000.3604	−5.2503	0.9108
1.30	.0257	0.	1.22	1.17	−2.51	2.40	8.04	7.69	6.59	6.57	6.58	7.89	1999.8361	4.5918	−0.8570
1.35	.0235	0.	1.06	1.03	−4.26	4.11	6.65	6.41	6.27	6.23	6.25	8.53	1998.7797	−0.8800	1.0304
1.40	.0226	0.	0.98	0.96	−5.34	5.18	5.94	5.76	6.06	6.00	6.03	9.01	1997.2714	−1.2851	1.0876
1.45	.0249	0.07	0.88	0.85	−6.51	6.26	5.23	5.02	5.94	5.91	5.59	9.87	1995.1786	−1.9478	1.0926
1.50	.0223	0.10	0.86	0.84	−7.03	6.80	5.07	4.91	5.90	5.85	5.28	10.70	1992.6348	−2.1173	1.4052
1.55	.0154	0.11	0.77	0.76	−7.91	7.71	4.55	4.43	5.90	5.83	4.79	12.50	1989.4268	−9.8654	1.7786
1.629	.0155	1.00	1.00	1.00	−6.52	6.41	6.52	6.41	6.52	6.41	0.0979	13.58	2009.7338	−9.0951	−0.3938
2.20	.0191	1.00	1.00	1.00	−11.05	10.87	6.56	6.45	6.56	6.45	0.00	22.7	1850.9216	−8.9159	0.3472

Table 10. An adiabatic interaction potential, $V(R)$, and ATCSM parameters for $^{272}_{110}$X using the asymmetric channel ^{64}Ni + ^{208}Pb. Here, the units of lengths and energies are in Fermi and MeV, respectively.

λ	η	ϵ	β_1	β_2	z_1	z_2	a_1	a_2	b_1	b_2	Neck	R_{cm}	V_{LDM}	δu	δp
1.20	.528	0.	1.58	0.66	−2.54	0.96	11.29	4.26	7.15	6.46	6.63	7.22	2003.1966	−3.1696	1.0538
1.25	.532	0.	1.64	0.69	−2.95	1.12	11.44	4.34	6.98	6.29	6.46	7.49	2002.6707	1.5155	0.0046
1.30	.532	0.	1.72	0.73	−3.18	1.21	11.76	4.48	6.84	6.14	6.31	7.84	2002.0402	4.5092	−1.1805
1.35	.523	0.	1.49	0.69	−5.45	2.20	9.81	3.97	6.59	5.75	5.96	8.55	2001.1486	2.4270	0.3195
1.40	.524	0.	1.39	0.69	−6.66	2.82	8.95	3.79	6.44	5.49	5.73	9.04	1999.9810	−0.6384	1.6370
1.45	.524	0.	1.25	0.63	−8.32	3.56	7.80	3.34	6.24	5.30	5.53	9.62	1998.2822	−1.9873	1.3318
1.50	.526	0.00	1.28	0.64	−8.88	3.78	7.83	3.33	6.11	5.20	5.43	10.00	1996.5785	−2.1045	0.9663
1.55	.536	0.00	1.18	0.55	−10.55	4.28	6.95	2.82	5.89	5.13	5.32	11.1	1994.5079	−2.3437	1.3969
1.589	.505	1.00	1.00	1.00	−7.53	5.08	7.53	5.08	7.53	5.08	0.0001	13.33	2026.8399	−9.8869	2.0347
2.40	.529	1.00	1.00	1.00	−15.13	10.22	7.61	5.14	7.61	5.14	0.00	25.90	1928.5531	8.0439	−1.5697

radius. The outer (second) turning point, R_f, is chosen such that $V(R_f) = V(R_i)$. Here, the reverse choice of the inner and the outer turning points is made on the basis of the principle of detailed balance.

We solve the integral in eq. (12) analytically. For this purpose, we parameterize the adiabatic interaction potential, $V(R)$, (fig. 3) between the inner and outer turning points by a second-order polynomial

$$V(R) = V_0 - bR + cR^2; \qquad R_i \le R \le R_f. \tag{13}$$

Here, the constants, V_0, b, c are real and positive. Thus, the transmission probability is given by

$$P_R = \exp\left[-\frac{2}{\hbar}\sqrt{2\mu}G\right], \tag{14}$$

with

$$G = \frac{1}{8c^{\frac{3}{2}}}\Big[2\sqrt{c}\Big(-(b+2cR_i)\sqrt{a+R_i(b+cR_i)} + (b+2cR_f)\sqrt{a+R_f(b+cR_f)}\Big) + (b^2-4ac)(T_1-T_2)\Big], \tag{15}$$

$$T_1 = \ln\left(\frac{b+2cR_i}{\sqrt{c}} + 2\sqrt{a+R_i(b+cR_i)}\right), \tag{16}$$

$$T_2 = \ln\left(\frac{b+2cR_f}{\sqrt{c}} + 2\sqrt{a+R_f(b+cR_f)}\right) \tag{17}$$

and $a = V_0 - V(R_i)$.

2.3 The fusion cross-section

Finally, the compound-nucleus formation cross-section is given by

$$\sigma = \pi\lambda\!\!\!^{-2} P_{CN} P_R\,, \tag{18}$$

where $\lambda\!\!\!^{-}$ is the de Broglie wavelength of the entrance channel. In eq. (18), both P_{CN} and P_R are normalized separately. Also, in the fusion process II, the $\pi\lambda\!\!\!^{-2}$ remain nearly constant. Therefore, in our calculations, we have chosen its value equal to 1 fm^2.

In this equation, we have not included the contribution of the summation over the angular momentum due to the following reasons.

Here, an angular momentum up to $\sim 20\hbar$ may contribute to the fusion cross-section [2]. Both, P_{CN} and P_R

depend on the angular momentum. An increase in angular momentum increases the E_{cm}, which suppresses the shell effects both in potential and mass parameters. This decrease in shell effects decreases the P_{CN} [11]. Also, the P_R is expected to decrease with the increase in angular momentum. This decrease in P_R can be understood from eq. (12), in which the contribution of rotational energy (a positive quantity) in the potential is added. Thus, the product $P_{CN} \times P_R$ decreases significantly with the increase in angular momentum. Therefore, in our present study, we have not included the contribution of higher angular-momentum summation terms.

3 Results and discussions

Here, we discuss the results of $^{256}_{102}$No in some detail; the results for other systems, namely, $^{258}_{104}$Rf, $^{260}_{106}$Sg, $^{266}_{108}$Hs and $^{272}_{110}$X are also given in a similar manner. Firstly, we search for appropriate channels for the compound-nucleus formation. The potential energy $V(\eta_Z)$ for the composite systems $^{256}_{102}$No is calculated by using eq. (7) and is shown by curve (a) in fig. 1. In these calculations, the nuclear shell effects, which are important in the fusion process II, are included through the experimental binding energies. Curve (b) in fig. 1, refers to the potential $V(\eta_Z)$ with $V_P = 0$, *i.e.* the sum of binding energies and the Coulomb energy terms. The comparison of curves (a) and (b) reveals that the inclusion of V_P does not bring any alteration in these minima, except that the minima at large charge asymmetry become slightly deeper. This evidently means that the potential energy minima are mainly due to the shell effects in the binding energies. Figure 1 shows two deep minima, one refers to the symmetric or nearly symmetric combination (*i.e.* ^{124}Sn + ^{132}Te), whereas the other corresponds to an asymmetric one (*i.e.* ^{48}Ca + ^{208}Pb). Here, we would like to point out that the large asymmetry region in the potential energy (*i.e.* ^{4}He + ^{252}Fm) is considered for cluster emission [24] and is, therefore, not suited for the compound-nucleus formation.

Similarly, the symmetric and the asymmetric channels for other four systems $^{258}_{104}$Rf, $^{260}_{106}$Sg, $^{266}_{108}$Hs and $^{272}_{110}$X are also seen in fig. 2, in which the potential, $V(\eta)$, is plotted *vs.* the mass asymmetry, η_A. Here, the proximity potential, V_P, is included. The symmetric and asymmetric channels for all these five systems ($Z = 102$–110 with $\Delta Z = 2$) are labeled in tables 1-10. From the following discussion, it is evident that only the asymmetric channels give rise to the fusion process II.

Next, we explore the relative importance of symmetric as well as asymmetric channels in the fusion process II. Complete fusion is the one in which target and projectile approach each other from $R = \infty$ and stick together before being tunneled. This implies that no conditional saddle is formed. In order to check this characteristic, we have calculated the adiabatic interaction potential, $V(R)$, for $Z = 102$ to $Z = 110$, in step of $\Delta Z = 2$, both for symmetric as well asymmetric channels (as obtained above) by carrying out a minimization of the total potential ($V_{LDM} + \delta u + \delta p$) in the ATCSM shape parameters

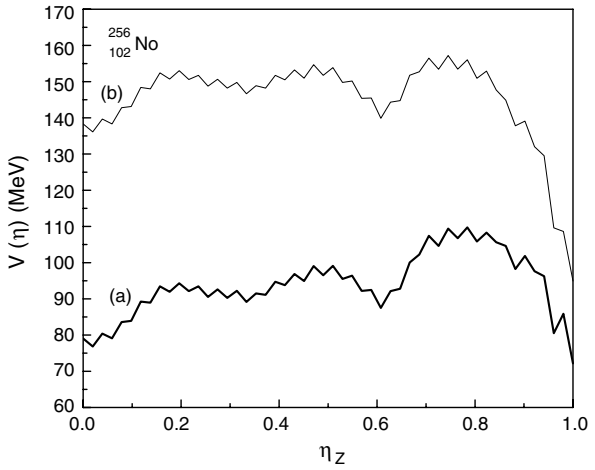

Fig. 1. (a) The potential $V(\eta)$ *vs.* the charge asymmetry, η_Z, for the system $^{256}_{102}$No is calculated by using eq. (7). (b) The potential with $V_P = 0$.

(β_i ($i = 1, 2$), ϵ and the dynamical mass asymmetry parameter, η_A) in a self-consistent manner. In these calculations, we have varied the elongation parameter λ from 2.40 to 1.20. The lower choice of the parameter λ (= 1.20) is enough to ensure complete fusion ($R_1 + R_2 \leq R_0$; R_0, being the radius of the compound nucleus). The interaction potential, $V(R)$, both for the asymmetric and the symmetric target and projectile combination are shown in figs. 3 and 4, respectively. We also have given the potential and the associated ATCSM shape parameters for all the five systems ($Z = 102$–110 with $\Delta Z = 2$) in tables 1-10. These values in the tables clearly show the shape evolution of the system from touching configuration to a complete overlap.

It is interesting enough to note from tables 1, 3, 5, 7 and 9 for the symmetric channels that a conditional saddle is formed at the elongation parameter $\lambda \sim 1.45$. The appearance of saddle shape implies that the memory of the incoming channel is still alive at such a large overlap (λ value 1.45). This observation contradicts the earlier hypothesis of the compound-nucleus formation [25]. This ruled-out possibility of the compound-nucleus formation is further confirmed from fig. 4, in which the interaction potential, $V(R)$, is plotted as a function of R_{cm}. Since the fusion barrier does not exist in any of the systems shown in this figure, its absence implies that the probability of forming the compound nucleus reduces to zero [11]. Recently, it has also been pointed out in ref. [26] that the symmetric combination leads to quasi-fission rather than to compound-nucleus formation.

On the other hand, we do not see any saddle shape in tables 2, 4, 6, 8 and 10. Also, the presence of a significant fusion barrier is clearly seen in each case of the asymmetric channels (see fig. 3). For example, the fusion barrier is seen for ^{48}Ca + ^{208}Pb $\rightarrow$ $^{256}_{102}$No at $R_B = 7.74$ fm. Thus, the asymmetric target-projectile combinations support the compound-nucleus formation through the fusion process II.

In this two-step process of "fusion following capture (touching)", we have extracted an estimate of the

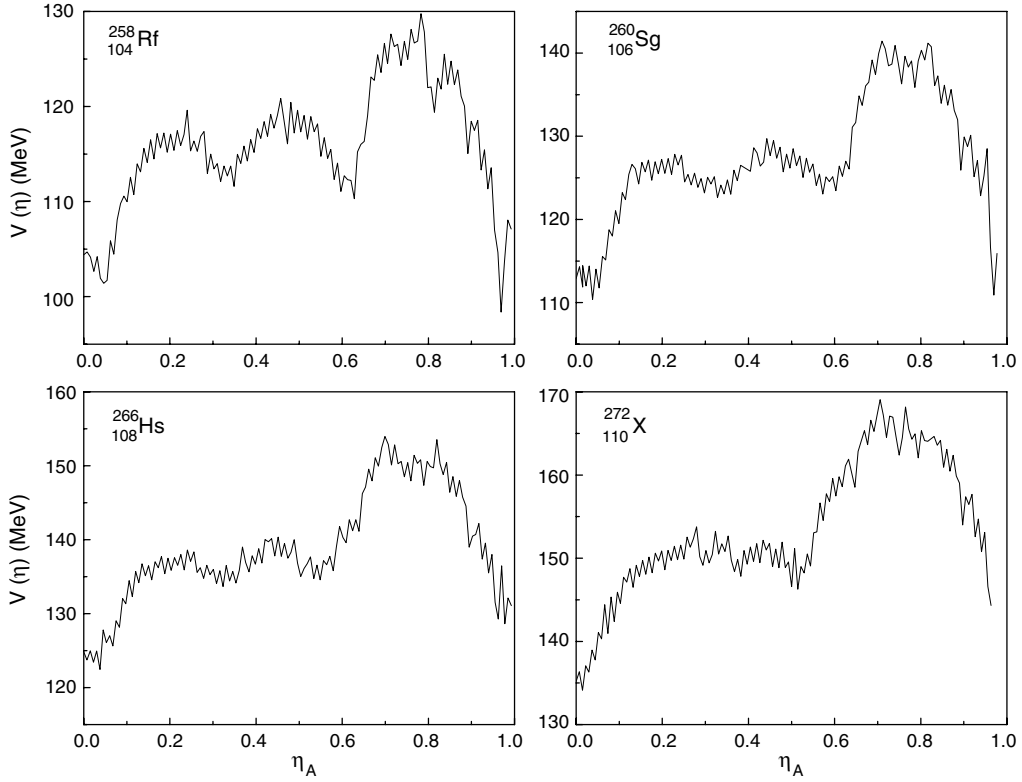

Fig. 2. The potentials $V(\eta)$ *vs.* the mass asymmetry, η_A, for the systems $^{258}_{104}$Rf, $^{260}_{106}$Sg, $^{266}_{108}$Hs and $^{272}_{110}$X are calculated by using eq. (7).

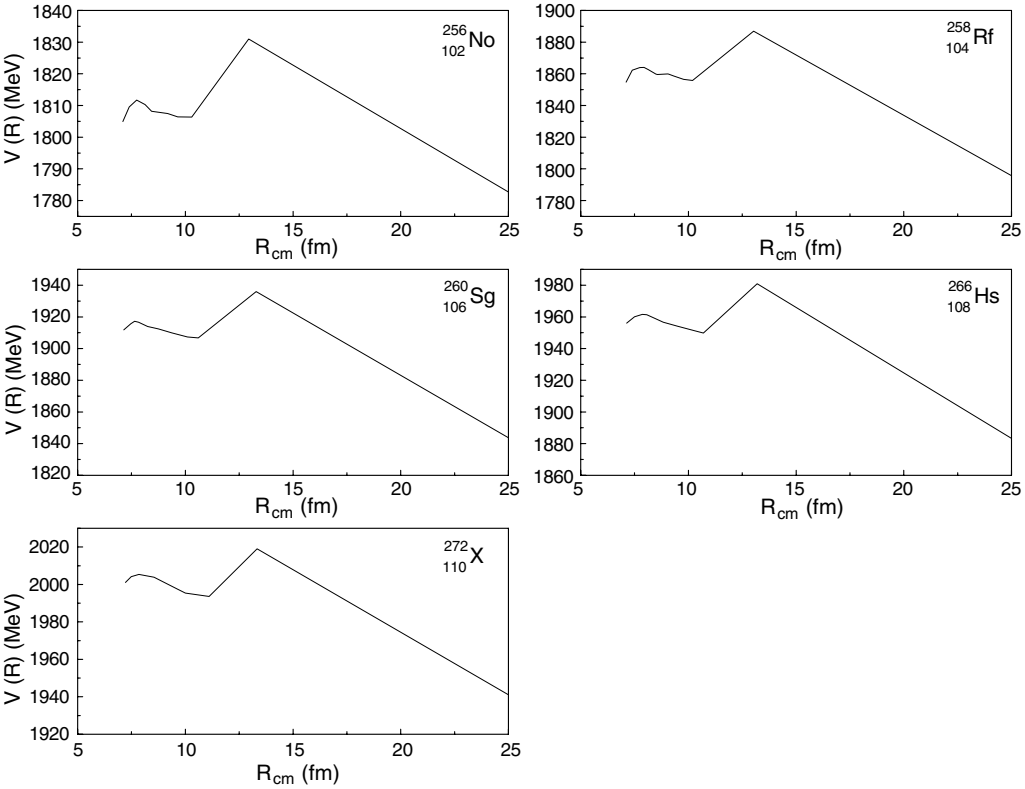

Fig. 3. The adiabatic interaction potential, $V(R)$, for the asymmetric target-projectile combinations $^{48}\mathrm{Ca} + ^{208}\mathrm{Pb} \rightarrow ^{256}_{102}\mathrm{No}$; $^{50}\mathrm{Ti} + ^{208}\mathrm{Pb} \rightarrow ^{258}_{104}\mathrm{Rf}$; $^{54}\mathrm{Cr} + ^{206}\mathrm{Pb} \rightarrow ^{260}_{106}\mathrm{Sg}$; $^{58}\mathrm{Fe} + ^{208}\mathrm{Pb} \rightarrow ^{266}_{108}\mathrm{Hs}$ and $^{64}\mathrm{Ni} + ^{208}\mathrm{Pb} \rightarrow ^{272}_{110}\mathrm{X}$.

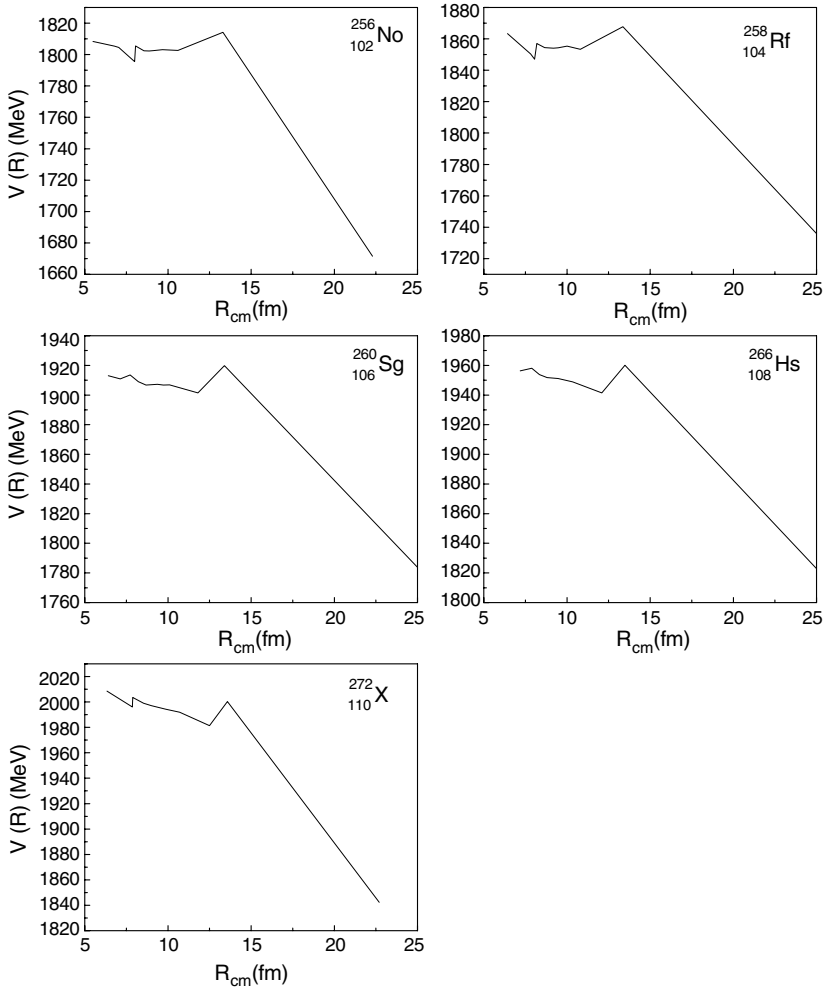

Fig. 4. The adiabatic interaction potential, $V(R)$, for the symmetric target-projectile combinations $^{124}\mathrm{Sn} + {}^{132}\mathrm{Te} \rightarrow {}^{256}_{102}\mathrm{No}$; $^{122}\mathrm{Sn} + {}^{136}\mathrm{Xe} \rightarrow {}^{258}_{104}\mathrm{Rf}$; $^{122}\mathrm{Sn} + {}^{138}\mathrm{Ba} \rightarrow {}^{260}_{106}\mathrm{Sg}$; $^{132}\mathrm{Xe} + {}^{134}\mathrm{Xe} \rightarrow {}^{266}_{108}\mathrm{Hs}$ and $^{132}\mathrm{Te} + {}^{140}\mathrm{Ce} \rightarrow {}^{272}_{110}\mathrm{X}$.

excitation energy carried by the compound nucleus. Here, the incoming system gets captured in the pocket behind the touching barrier (fig. 3), before being tunneled through the fusion barrier. This pocket in the potential energy curve refers to the stable equilibrium position of the captured system and its energy value may be considered equivalent to the ground state of the compound nucleus. It is interesting to note that the values of R_{cm} at the pocket position are nearly equal to the touching distance between the two fragments. The excitation energy of the compound nucleus, E^*, is defined as the height of the barrier measured from its ground state. We have chosen this height equal to that of the outer-barrier height. This quantity is calculated by taking the difference between the top and bottom values of the barrier and they are are given in table 11. Since it is a relative difference between the two values, it is independent of the choice of the parameters used in our model. The experimental values of E^* are also given in this table. A comparison between the calculated and experimental values reveal that the calculated values are higher by 8–15 MeV in all the five systems. It is worth mentioning here that one of the reasons for this difference is that we have not considered any angular-momentum contribution in our calculations. An increase in angular momentum decreases the height of the barrier [11] and thus the excitation energy decreases.

Further, we have calculated the preformation probability, P_{CN}, for $^{256}_{102}$No by using the potential shown by curve (a) in fig. 1. We use the model of Kroger and Scheid [20] for the mass parameters, $B_{\eta_Z \eta_Z}$. The normalized yield, P_{CN}, *vs.* the charge number, Z, is shown in fig. 5. Here, we have taken only the ground-state contribution, as the excitation energy of the system $^{256}_{102}$No is quite small (see table 11). The peaks corresponding to the asymmetric channel $^{48}\mathrm{Ca} + {}^{208}\mathrm{Pb} \rightarrow {}^{256}_{102}\mathrm{No}$ in the normalized P_{CN} appear along with the symmetric channel $^{124}\mathrm{Sn} + {}^{132}\mathrm{Te} \rightarrow {}^{256}_{102}\mathrm{No}$. It is interesting enough to note that the touching probability, P_{CN}, for the symmetric channel is twice as large as that of an asymmetric channel, even though the symmetric channel does not form the compound nucleus (as discussed below). We have calculated the P_{CN} for the other four systems $^{258}_{104}$Rf, $^{260}_{106}$Sg, $^{266}_{108}$Hs and $^{272}_{110}$X by using their potential (fig. 2) together with the classical mass parameters. It is noticed that the behavior and magnitude of P_{CN} for all these five systems are nearly the same. A nearly identical behavior

Table 11. An estimation of threshold energy for the compound-nucleus reaction from the adiabatic interaction potential, $V(R)$.

Reaction	E^*_{cal} (MeV)	E^*_{exp} (MeV)	Q value (MeV)	E_{cm} (MeV)
$^{48}\mathrm{Ca} + {}^{208}\mathrm{Pb} \rightarrow {}^{256}_{102}\mathrm{No}$	24.6465	16.0	153.796	178.4425
$^{50}\mathrm{Ti} + {}^{208}\mathrm{Pb} \rightarrow {}^{258}_{104}\mathrm{Rf}$	31.1308	15.0	169.69	200.8208
$^{54}\mathrm{Cr} + {}^{206}\mathrm{Pb} \rightarrow {}^{260}_{106}\mathrm{Sg}$	29.2444	15.0	187.33	216.5744
$^{58}\mathrm{Fe} + {}^{208}\mathrm{Pb} \rightarrow {}^{266}_{108}\mathrm{Hs}$	31.0694	14.0	205.01	236.0794
$^{64}\mathrm{Ni} + {}^{208}\mathrm{Pb} \rightarrow {}^{272}_{110}\mathrm{X}$	25.4299	12.2	225.16	250.5899

Table 12. Fitted potential parameters (in MeV), the penetration probability, P_R, compound-nucleus cross-sections using asymmetric channels. Here, P_{CN} is taken as 2.555×10^{-2}. The experimental values of the cross-section are also given.

Nucleus	V_0	b	c	$V(R_i)$	P_R	σ_{cal} (fm^2)	σ_{exp} (fm^2)
$^{256}_{102}$No	1910.43	20.8142	1.0405	1806.3526	8.0466×10^{-4}	2.0559×10^{-5}	$1.3 \pm 0.4 \times 10^{-5}$
$^{258}_{104}$Rf	1925.14	−11.3152	0.4437	11855.7559	1.7761×10^{-5}	4.538×10^{-7}	$1.0 \pm 0.13 \times 10^{-6}$
$^{260}_{106}$Sg	1990.74	−13.9139	0.5635	1906.7493	9.9647×10^{-8}	2.546×10^{-9}	$5.0 \pm 1.4 \times 10^{-8}$
$^{266}_{108}$Hs	2036.60	−13.3493	0.4905	1949.8572	1.2518×10^{-8}	3.1982×10^{-10}	$6.7 \pm 0.75 \times 10^{-9}$
$^{272}_{110}$X	2071.03	−11.2815	0.3837	1993.5578	7.4068×10^{-10}	1.8924×10^{-11}	$1.5 \pm 0.9 \times 10^{-9}$

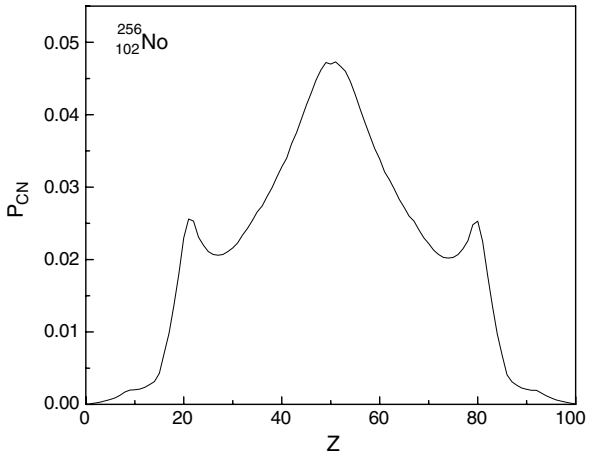

Fig. 5. The normalized compound-nucleus preformation probability, P_{CN}, as a function of Z for a composite system $^{256}_{102}$No with the V_P contribution in the potential energy.

arises due to the absence of shell effects in the mass parameters and it does not explain the observed behavior of the cross-section. One must use the ATCSM states in the adiabatic cranking formula for obtaining the mass parameters [11,27]. This involves a lot of computational work and hence these latter are not calculated here.

The tunneling probability, P_R, is calculated by using the analytical expressions (14)-(17). Here, the ATCSM potentials (fig. 3) are fitted by the second-order polynomial of eq. (13). The fitted potential parameters for the five systems (Z = 102–110 with $\Delta Z = 2$) are given in table 12. The limits of integration in eq. (12) are chosen from the compound-nucleus radius to the pocket position (touching configuration). The calculated P_R values are given in this table. We have calculated the fusion cross-section by using eq. (18) with constant value of P_{CN} ($= 2.555 \times 10^{-2}$, *i.e.* the value of $^{48}\mathrm{Ca} + {}^{208}\mathrm{Pb} \rightarrow {}^{256}_{102}\mathrm{No}$). In table 12, both the calculated and experimental values of the cross-sections are given. The experimental cross-sections, given in this table, are one-neutron evaporation residue cross-section. We notice that our calculated cross-section for $^{48}\mathrm{Ca} + {}^{208}\mathrm{Pb} \rightarrow {}^{256}_{102}\mathrm{No}$ compares reasonably well with the measured value. However, the calculated values for the other four systems are off by a factor of 10 of the experimental data.

It is remarkable to notice in table 12 that the behavior of the calculated P_R is fairly in agreement with the experimental cross-section. Here, we would like to point out that this nice comparison arises due to the total minimization of the potential by using the ATCSM. If we extract the P_{CN} values ($= \frac{\sigma_{exp}}{P_R}$), it shows an increasing trend with the increase in size of the projectile. This behavior favors our result (fig. 5) that the symmetric channel has larger P_{CN} than an asymmetric channel. Another interesting point to note here is that an extracted value of the P_{CN} for $^{48}\mathrm{Ca} + {}^{208}\mathrm{Pb} \rightarrow {}^{256}_{102}\mathrm{No}$ ($= 1.6156 \times 10^{-2}$) is reasonably close to our calculated value ($= 2.555 \times 10^{-2}$). These calculations of the P_{CN} certainly need an improvement by using the cranking mass parameters.

In our model, we have realized the importance of P_R. However, the fusion barriers are completely absent in the symmetric-channel cases (fig. 4). Therefore, the limits of the integration (*i.e.* the termination points) in eq. (12) are shifted to 0 and ∞ ($\sim$ 25 fm). Within these limits, P_R reduces to zero and hence the probability of forming the compound nucleus vanishes. Therefore, in case of symmetric channels, the appearance of a conditional saddle and the absence of the fusion barrier force the system to quasi-fission rather than forming the compound nucleus. These conclusions are consistent with the recent observations of ref. [26].

4 Conclusions

Here, we have shown that the asymmetric minima in the potential energy curves reproduce the experimentally known channels for the compound-nucleus formation. This technique, therefore, appears to be quite useful to predict the channels for the production of new upcoming heavy and superheavy nuclei. Our model calculations are also able to give an estimate of the threshold energy for the fusion process II. The existence of a fusion barrier is a must for the formation of the compound nucleus. The shell effects in the potential and mass parameters appear to play an important role in the fusion process II. The calculated fusion cross-sections yield reasonably well the observed one-neutron evaporation residue cross-section. However, further refinements in the model are needed and are underway.

This work is supported by the Department of Science and Technology, University Grants Commission and Department of Atomic Energy (Government of India). We would like to thank the referee for fruitful comments and suggestions

References

1. S. Hofmann, Rep. Prog. Phys. **61**, 639 (1998).
2. S. Hofmann, G. Munzenberg, Rev. Mod. Phys. **72**, 733 (2000).
3. P. Armbruster, Annu. Rev. Nucl. Part. Sci. **50**, 411 (2000).
4. Ch.E. Dullmann *et al.*, Nature **418**, 859 (2002).
5. S. Hofmann *et al.*, Eur. Phys. J. A **10**, 5 (2001).
6. Yu.Ts. Oganessian *et al.*, Eur. Phys. J. A **5**, 68 (1999); Phys. Rev. Lett. **83**, 3154 (1999); Nature **400**, 209 (1999); Phys. Rev. C **62**, 041604(R) (2000); **63**, 011301(R) (2001); Eur. Phys. J. A **15**, 201 (2002).
7. H.J. Fink *et al.*, *Proceedings of the International Conference on Reactions between Complex Nuclei, Nashville, June 1974*, Vol. **2** (North Holland, Amsterdam, 1974) p. 21.
8. A. Sandulescu, R.K. Gupta, W. Scheid, W. Greiner, Phys. Lett. B **60**, 225 (1976).
9. R.K. Gupta, A. Sandulescu, W. Greiner, Phys. Lett. B **67**, 217 (1977).
10. R.K. Gupta, C. Parvulescu, A. Sandulescu, W. Greiner, Z. Phys. A **283**, 217 (1977).
11. R. Aroumougame, N. Malhotra, S.S. Malik, R.K. Gupta, Phys. Rev. C **35**, 994 (1987).
12. W. Greiner, R.K. Gupta (Editors), *Heavy Elements and Related New Phenomena* (World Scientific Publ., 1999).
13. Caiwan Shen, Grigori Kosenko, Yasuhisa Abe, Phys. Rev. C **66**, 061602 (2002).
14. D.R. Saroha, R.K. Gupta, J. Phys. G **12**, 1265 (1986).
15. S.S. Malik, N. Malhotra, D.R. Saroha, R.K. Gupta, International Centre for Theoretical Physics, Trieste, Italy, Report No. IC/86/128.
16. J. Maruhn, W. Greiner, Z. Phys. **251**, 431 (1972).
17. F. Caitucoli, M. Asghar, G. Barreau, B. Leroux, P. Perrin, M. Maurel, T.P. Doan, A. Sicre, in *Proceedings of the International Conference on Nuclear Data for Basic and Applied Science, Sante Fe, NM, 13-17 May, 1985* (Gordon and Breach Science Publ., 1986).
18. G. Audi, A.H. Wapstra, G. Thibalt, Nucl. Phys. A **729**, 337 (2003).
19. J. Blocki, J. Randrup, W.J. Swiatecki, C.F. Tsang, Ann. Phys. (N.Y.) **105**, 427 (1977).
20. H. Kroger, W. Scheid, J. Phys. G **6**, L85 (1980).
21. S. Yamaji, W. Scheid, H.J. Fink, W. Greiner, J. Phys. G **3**, 1283 (1977).
22. K.J. Le Cauteur, W.D. Lang, Nucl. Phys. **13**, 32 (1959).
23. W.D. Myers, W.J. Swiatecki, Ark. Fys. **36**, 343 (1967).
24. S.S. Malik, R.K. Gupta, Phys. Rev. C **39**, 1992 (1989).
25. S.N. Ghosal, Phys. Rev. **80**, 939 (1950).
26. G.G. Adamian, N.V. Antonenko, S.P. Ivanova, W. Scheid, Nucl. Phys. A **646**, 29 (1999).
27. D.R. Inglis, Phys. Rev. **96**, 1059 (1959); S.T. Balyaev, Kgl. Dansk. Vidensk. Sels. Mat.-Fys. Medd. **31**, No. 11 (1959).